Dental Materials Journal 2010; 29(1): 35–40

Radio-opacity of core materials for all-ceramic restorations

Yuji OKUDA[1], Makoto NODA[1], Hiroshi KONO[2], Motoharu MIYAMOTO[3], Hideo SATO[4] and Seiji BAN[1]

[1]Department of Biomaterials Science, [2]Department of General Dental Clinic, [3]Department of Dental Radiology, and [4]Department of Pediatric Dentistry, Graduate School of Medical and Dental Sciences, Kagoshima University, 8-35-1 Sakuragaoka, Kagoshima 890-8544, Japan
Corresponding author, Yuji OKUDA; E-mail: k2357241@kadai.jp

The aim of this study was to investigate and compare the radio-opacity of core materials for all-ceramic restorations, such as zirconia (NANOZR and Y-TZP) and alumina, against commercially pure titanium (cpTi) and aluminum. X-ray images were taken under general settings using an X-ray film. The X-ray film images were scanned using a digital scanner, and the darkness at the central area of each specimen image was quantitatively analyzed using an image analysis software. Amongst the materials investigated, alumina showed the most transparency against X-rays. Conversely, both types of zirconia showed the highest radio-opacity, whereby that of NANOZR was slightly lower than that of Y-TZP. This was because NANOZR contained 30 vol% of alumina and its density was also slightly lower than that of Y-TZP.

Keywords: Radio-opacity, Zirconia, Alumina

Received Jul 2, 2009: Accepted Sep 11, 2009

INTRODUCTION

High-strength ceramics such as zirconia and alumina are widely used as dental restorative materials. In particular, 3 mol% yttria-stabilized tetragonal zirconia polycrystals (Y-TZP) have been increasingly used for dental crowns and bridges[1]. This is because Y-TZP has several advantages that befit its use as a dental restorative material: good chemical and dimensional stability, high mechanical strength and toughness, and a Young's modulus which is within the same order of magnitude as stainless steel alloys[2-4].

Exploiting the advances in nanotechnology, Nawa *et al*. developed a tough and strong ceria-stabilized tetragonal zirconia polycrystal (Ce-TZP)/Al_2O_3 nanocomposite, known as NANOZR, in 1998[5]. This material had an interpenetrated intragranular nanostructure, in which either nanometer-sized Ce-TZP or Al_2O_3 particles were located within submicron-sized Al_2O_3 or Ce-TZP grains respectively. The design of this material made it possible to strengthen the 10 mol% ceria-stabilized TZP matrix with 30 vol% Al_2O_3. Upon comparing this novel material with Y-TZP, it was found that NANOZR was significantly stronger than Y-TZP and that no low-temperature aging degradation (LTAD) was observed after soaking in aqueous solutions[6,7].

In terms of application potential, zirconia ceramics may also be used for implant fixtures[8]. In light of their varied and versatile application potential, various bioactive surface modification methods have been applied on zirconia in this decade[9-11].

Despite the considerable interest in and increasing popularity of all-ceramic dental restorations, no rigorous research has been conducted on the radio-opacity of these ceramic materials to date. It is noteworthy that radio-opacity is an indispensable property for dental restorative materials during clinical diagnosis, which in turn depends heavily on radiology. To identify and distinguish an intraorally placed material, such as a resin or cement, from surrounding anatomical structures, the radio-opacity of the material must be sufficiently different from that of tooth tissue to be discriminated; but at the same time, it must be radio-opaque enough to be distinguished from a void.

The aim of this study was to investigate the radio-opacity of two types of ceramics, zirconia and alumina, and compare them against commercially pure titanium — which is widely used as a dental implant material, and against aluminum — which is used as a standard to measure relative radio-opacity in an *ex vivo* setting. Thereafter, in light of this study's results, discussion would focus on the possibility of identifying and discriminating intraorally placed all-ceramic dental restorations.

MATERIALS AND METHODS

Table 1 lists the product names and manufacturers of the materials used in this study. The thicknesses of the specimens prepared from each material were also listed in this table.

Specimen preparation

The powders of NANOZR, Y-TZP, and alumina were pressed into a cylindrical rod using cold isostatic pressing (CIP) under 245 MPa for 1 minute. The pressed rods were subsequently pre-sintered at 850°C for 2 hours at a heating rate of 1°C/minute. Finally, they were sintered at 1,450°C for 2 hours, at 1,350°C for 6 hours, and at 1,500°C for 2 hours, respectively. After the final firing, the rods were cut to various thicknesses with a 400-grit diamond wheel. For cpTi specimens, they were cut from the commercial plate. In total, 29 plate-like specimens were thus prepared. An aluminum step-wedge with a thickness range of 1 mm to 16 mm, whereby thickness increased by 1 mm per step, was used as the control specimen.

Table 1 Materials used in this study

Code	Material	Thickness (mm)
Y-TZP	3 mol% yttria-stabilized tetragonal zirconia polycrystals (TZ-3YB-E, Tosoh, Yamaguchi, Japan)	0.1, 0.2, 0.3, 0.5, 1.0, 1.2, and 1.94
NANOZR	Ceria-stabilized tetragonal zirconia polycrystals (Ce-TZP)/Al_2O_3 nanocomposite (MACZ-100, Panasonic Electric Works, Osaka, Japan)	0.1, 0.2, 0.3, 0.4, 0.5, 0.6 0.7 0.8, 0.9, 1.0, 1.2, and 1.9
Alumina	Pure alumina (TM-DA, Taimei Chemical, Nagano, Japan)	0.1, 0.3, 0.5, 1.2, and 1.95
cpTi	Commercially pure titanium (TI-453382, TI-453441, and TI-453460, Nilaco, Tokyo, Japan, and KS-50, KOBELCO, Hyogo, Japan)	0.2, 0.4, and 0.5 (Nilaco), 1.0, and 2.0 (KOBELCO)
Aluminum	Pure aluminum (a custom-made item)	1–8 and 8–16 in steps of 1 mm

Table 2 Film combinations used in this study to obtain the X-ray images of specimens

Material	Film 1	Film 2	Film 3	Film 4
Y-TZP	–	0.2, 0.5, 1.0, and 1.94 mm	0.1, 0.3, 0.5, and 1.2 mm	–
NANOZR	0.1–1.0 in steps of 0.1 mm	0.2, 0.5, 1.0, and 1.9 mm	0.1, 0.3, 0.5, and 1.2 mm	0.1, 0.3, 0.5, and 1.2 mm
Alumina	–	0.5 and 2.0 mm	0.1, 0.3, 0.5, and 1.2 mm	0.1, 0.3, 0.5, and 1.2 mm
cpTi	1.0 mm	0.2, 0.5, 1.0, and 2.0 mm	0.2, 0.4, 1.0, and 2.0 mm	0.2, 0.4, 1.0, and 2.0 mm
Aluminum	–	–	1–16 in steps of 1 mm	–

Grain size determination using SEM

Apparent grain size (D) was determined using the lineal intercept method[12] from the SEM photographs of these surfaces: thermally etched surfaces of both types of zirconia and alumina and the chemically etched surface of cpTi. The following equation was then used for grain size determination:

$$D = 1.56\ C / M / \mathrm{N} \quad (1)$$

where C is the total length of test line used, N the number of intercepts, and M the magnification of the photomicrograph. The proportionality constant, 1.56, was essentially a correction factor which was derived by Menderson[13] for random slices through a model system consisting of space-filling tetrakaidecahedrally shaped grains with a log-normal size distribution. In the case of NANOZR, each grain size of Ce-TZP and Al_2O_3 was also determined.

X-ray images

X-ray images were obtained using an X-ray unit (MAX F-1, Morita Co., Tokyo, Japan) with Kodak DF49 film under these settings: 60 kV, 10 mA, and at 40 cm for 0.90 seconds. The films were developed, fixed, and dried in an automatic processor (XR 24 Nova, Dürr-Dental, Dürr, Bietigheim-Bissingen, Germany). The image developer (RD-1B, Fuji, Tokyo, Japan) was maintained at 28.6°C, and total processing time was 5.5 minutes.

The developed X-ray image films were scanned using a digital scanner (CanoScan 8600F, Canon, Tokyo, Japan), and the darkness at the central area of each specimen image was quantitatively analyzed using an image analysis software (Scion Image 1.63, Maryland, USA). For each specimen, its optical density was derived from the darkness of the specimen image to the background. As one sheet of film could not cover all the X-ray images of all the specimens, the specimens were divided to four combinations as listed in Table 2. Three films were used for each combination. To compensate for incorrect exposure during the X-ray film development procedure, darkness of the background and 1.0-mm-thick cpTi were used as standard values for calibration. The equivalent thickness of aluminum (in mm) was derived from the apparent absorption coefficients, whereby the latter were calculated from the linear regression of the logarithm of the average optical density of the test specimen and its thickness compared to that in the image of the aluminum step wedge. Aluminum has been widely used as a radiographic standard, and the use of an aluminum step wedge of at least 98 mass% purity is specified in the current ISO standard for polymer-based filling, restorative, and luting materials (ISO-4049: 2000)[14].

ISO and ADA are existing protocols for determining radio-opacity using film-based radiography. Based on

the existing protocols, the radio-opacity of a 1.0-mm-thick specimen was to be determined from the optical density of an X-ray image of the specimen as the equivalent thickness of aluminum by referring to an image of an aluminum step wedge. The thickness value adopted should be the nearest higher value of thickness from the aluminum step wedge. According to ISO 4049 7.14:2000[14] and ISO 9917-1 Annex H:2007[15], it was commented that the accuracy of this determination method could be improved by plotting optical density against the aluminum thickness of the step wedge for each radiographic exposure. In the present study, the equivalent thickness of aluminum (in mm) was derived from the attenuation coefficients, which were calculated from the linear regression of the logarithm of optical density against the thickness for the specimen.

RESULTS

Figure 1 shows the SEM photographs of the test specimens. Y-TZP, alumina, and cpTi consisted of homogeneous grains, with average grain sizes of 0.32±0.10, 2.42±0.22, and 27.0±3.1 μm respectively. NANOZR was composed of 10 mol% CeO_2-stabilized TZP (white grains) as a matrix and 30 vol% of Al_2O_3 (black grains) as a second phase. The average grain size of both phases indiscriminately was 0.49±0.12 μm. Upon individual grain size determination for each phase, the grain sizes of Ce-TZP and Al_2O_3 were 0.59±0.09 μm and 0.42±0.08 μm respectively. With NANOZR, a significant characteristic of its structure lay in its intragranular nanostructure, in which several 10–100 nm sized Al_2O_3 particles were trapped within the ZrO_2 grains and *vice versa*, several 10-nm sized ZrO_2 particles were trapped within the Al_2O_3 grains.

Figure 2 shows the typical X-ray images of the test specimens obtained *via* the Film 3 combination listed in Table 2. The alumina plates showed the most transparency against X-rays. Conversely, the 1.2-mm specimens of both Y-TZP and NANOZR showed the highest opacity. Figure 3 shows the logarithm of X-ray optical density (I/I_0) of the specimens as a function of thickness. It was assumed that the attenuation coefficient (μ) consisted of the mass absorption (μ_{abs}) and scattering ($\mu_{scatter}$) coefficients as follows:

$$\mu = \mu_{abs} + \mu_{scatter} \quad (2)$$

For X-radiation in a medium, Lambert's Law applies as follows:

$$I = I_0 e^{-\mu x} \quad (3)$$

where I_0 is the (top surface) irradiance and I is the value at depth x.

From the regression curve with a function of I =

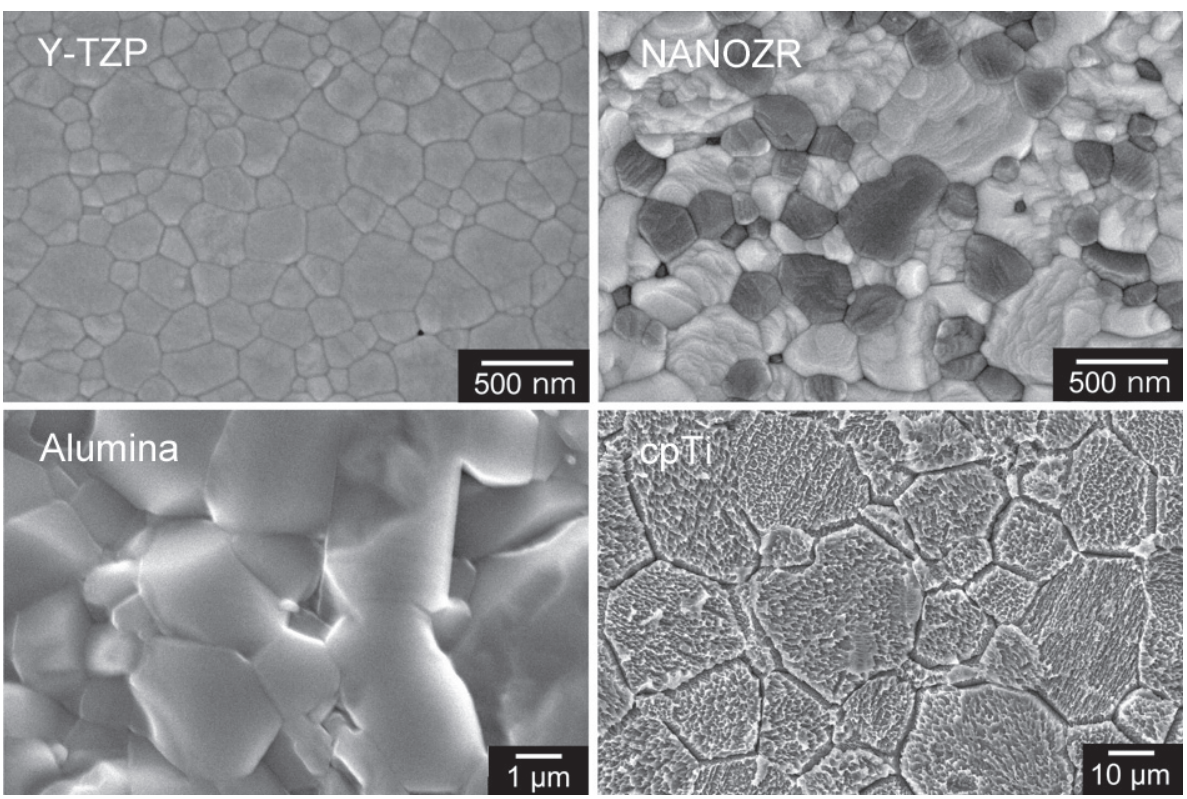

Fig. 1 SEM photographs of the surfaces of NANOZR, Y-TZP, alumina, and cpTi used in this study.

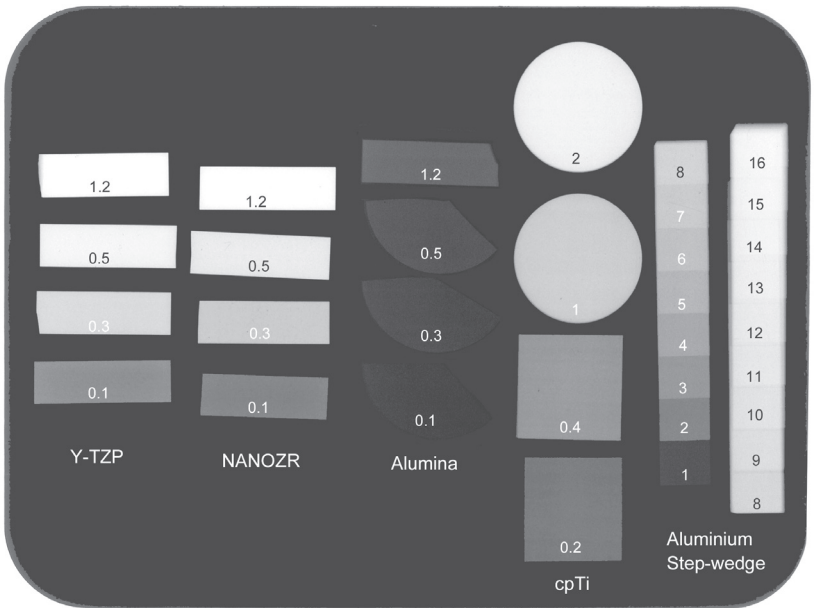

Fig. 2 Typical X-ray images of the test specimens obtained using Film 3 combination. Each numerical value indicates the specimen thickness in mm.

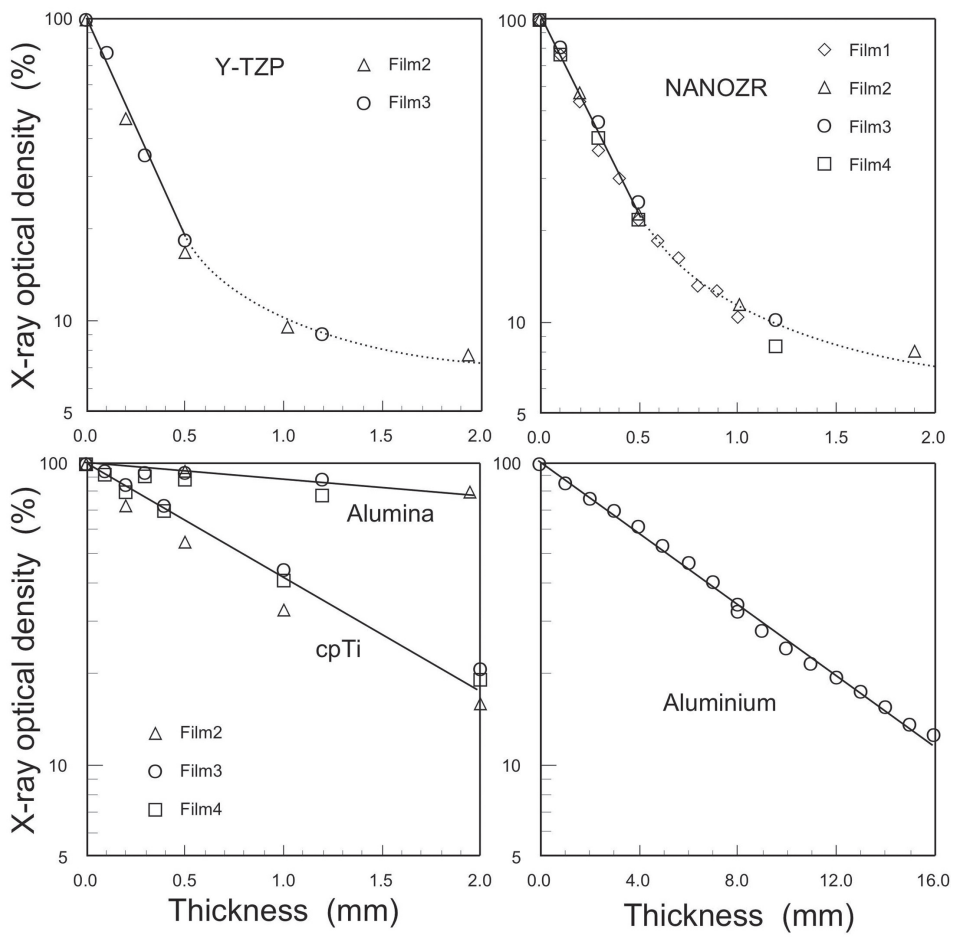

Fig. 3 Logarithm of X-ray optical density of NANOZR, Y-TZP, alumina, cpTi, and aluminum as a function of thickness. Each line represents the regression line from 0 to 0.5 mm for Y-TZP and NANOZR, from 0 to 2 mm for cpTi and alumina, and from 0 to 16 mm for aluminum.

$I_0e^{-\mu x}$, the attenuation coefficients were derived from the data in the thickness range <0.5 mm of both NANOZR and Y-TZP, and <2.0 mm of Ti because thicker specimens showed the saturated values. Following the X-ray exposure for Y-TZP, NANOZR, cpTi, alumina, and the aluminum step wedge, their corresponding attenuation coefficients and equivalent thicknesses of aluminum are given in Table 3. Based on the results shown, the radio-opacity of the tested materials could be ranked in the following descending order: Y-TZP > NANOZR >> Ti >> aluminum > alumina.

DISCUSSION

Radio-opacity is not only a desirable property for most dental materials, but that it is certainly indispensable for restorative materials for clinical diagnosis. As it is essential to be able to intuitively distinguish the denture base or dental restorative materials from tooth tissue, radio-opaque agents are sometimes added to these materials to obtain better radio-opacity[16-18].

As shown in Equation (2), radio-opacity depends on the absorption and scattering of X-rays by a material. On X-ray absorption in solid materials, it is chiefly due to photoelectric absorption; on the scattering of X-rays, it is caused by the effects of Thomson scattering and Compton scattering.

In the present study, it was assumed that photoelectric absorption accounted for the majority of X-ray interactions because of two reasons. First, the effective energy of dental X-rays was less than 30 keV. Secondly, Fig. 1 revealed the grain sizes of the tested materials to be 0.3–27.0 μm. These grain size dimensions were markedly greater than the X-ray wavelength range (about 0.02–0.008 nm), which meant that X-ray scattering was almost negligible.

On the order of radio-opacity obtained in this study, it could be attributed to the atomic number order of the component element in each material: oxygen 8; aluminum 13; titanium 22; yttrium 39; zirconium 40; and cerium 58. Alumina showed a high transparency against X-rays because it consisted of aluminum and oxygen with small atomic number. As for NANOZR, its radio-opacity was slightly lower than that of Y-TZP because NANOZR contained 30 vol% of alumina and its density was also slightly lower than that of Y-TZP.

Effective atomic number is a term that is similar to atomic number but is used for compounds and mixtures of different materials (such as Y-TZP and NANOZR) than for atoms. The formula for effective atomic number, Z_{eff}, is as follows[19]:

$$Z_{eff} = [f_1(Z_1)^{2.94} + f_2(Z_2)^{2.94} + f_3(Z_3)^{2.94} + \quad]^{1/2.94} \tag{4}$$

where f_n is the fraction of the total number of electrons associated with each element and Z_n is the atomic number of each element. Table 4 shows the composition and Z_{eff} of each tested material.

Pertaining to the attenuation coefficient (μ), it is induced by photoelectric absorption and is dependent on effective atomic number (Z_{eff}) and density (ρ) as follows[20]:

$$\mu \propto Z_{eff}^3 \rho \tag{5}$$

Figure 4 then shows the relation between the experimentally obtained μ derived from Fig. 3 and the calculated $Z_{eff}^3\rho$ of the materials tested in this study. A strong correlation, as attested by a straight line, was observed. This meant that the radio-opacity

Table 3 Radio-opacity determined as attenuation coefficients and equivalent thicknesses of aluminum

Material	Attenuation coefficient (mm^{-1})	Equivalent thickness of Al (mm)
Y-TZP	3.48	26.8
NANOZR	2.98	22.9
cpTi	0.83	6.4
Alumina	0.11	0.8
Aluminum	0.13	1.0

Table 4 Compositions of the materials tested and their effective atomic numbers

Material	Composition (f)						Z_{eff}	ρ (g/cm^3)	$Z_{eff}^3\rho$
	$_8$O	$_{13}$Al	$_{22}$Ti	$_{39}$Y	$_{40}$Zr	$_{58}$Ce			
Y-TZP	0.283			0.040	0.676		35.697	6.1	2.77×10^5
NANOZR	0.332	0.140			0.454	0.073	35.077	5.5	2.37×10^5
Alumina	0.600	0.400					8.778	3.9	2.64×10^3
cpTi			1.000				22.000	4.5	4.79×10^4
Aluminum		1.000					13.000	2.7	5.93×10^3

The values of ρ were quoted from Refs.6 and 21.

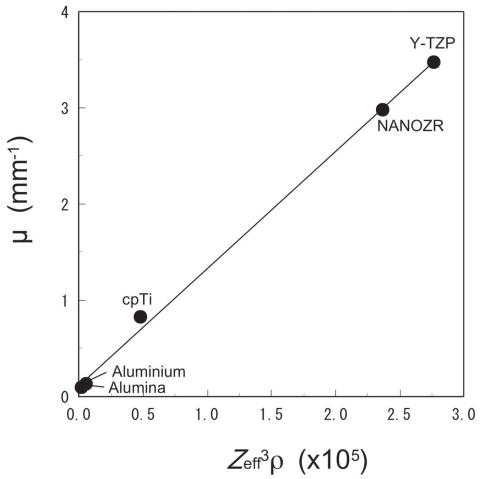

Fig. 4 Relation between the experimentally obtained X-ray attenuation coefficient (μ) and the calculated $Z_{eff}{}^3\rho$.

measurements obtained in the present study were valid because correct compositions were used in all the composite specimens. In other words, the composition of a composite could be estimated from a radio-opacity measurement.

Results of this study demonstrated that the radio-opacity of dental ceramics and metals strongly depended on photoelectric absorption under the general conditions of dental roentgenography. For this reason, zirconia exhibited a strong radio-opacity stemming from its high effective atomic number and density. This also meant that high-contrast roentgenographic images could be obtained for dental diagnosis if zirconia were to be used as a dental restorative.

CONCLUSIONS

Zirconia showed higher radio-opacity than titanium and aluminum. Between the two types of zirconia, the radio-opacity of NANOZR was slightly lower than that of Y-TZP. This was because NANOZR contained 30 vol% of alumina and its density was also slightly lower than that of Y-TZP. It was concluded that the radio-opacity of dental ceramics and metals strongly depended on photoelectric absorption under the general conditions of dental roentgenography. On this premise, zirconia exhibited high radio-opacity because of its inherently high effective atomic number and density, whereby high-contrast roentgenographic images could be obtained for dental diagnosis when it is used as a dental restorative.

ACKNOWLEDGMENTS

The present study was supported by a Grant-in-Aid for General Science Research (B-18390521) from the Japan Society for the Promotion of Science. The authors would also like to thank Panasonic Electric Works Co. Ltd. for kindly providing the zirconia specimens.

REFERENCES

1) Ban S. Reliability and properties of core materials for all-ceramic dental restoration. Japan Dent Sci Rev 2008; 44: 3-21.
2) Garvie RC, Haaink RH, Pascoe RT. Ceramic steel? Nature 1975; 258: 703-704.
3) Drummond JL. *In vitro* aging of yttria-stabilized zirconia. J Am Ceram Soc 1989; 72: 675–676.
4) Piconi C, Maccauro G. Zirconia as a ceramic biomaterial. Biomaterials 1999; 20: 1-25.
5) Nawa M, Nakamoto S, Sekino T, Niihara K. Tough and strong Ce-TZP/alumina nanocomposites doped with titania. Ceramic Int 1998; 24: 497-506.
6) Ban S, Sato H, Suehiro Y, Nakanishi H, Nawa M. Biaxial flexure strength and low temperature degradation of Ce-TZP/Al_2O_3 nanocomposite and Y-TZP as dental restoratives. J Biomed Mater Res B 2008; 87: 492-498.
7) Sato H, Yamada K, Pezzotti G, Nawa M, Ban S. Mechanical properties of dental zirconia ceramics changed with sandblasting and heat treatment. Dent Mater J 2008; 27: 408-414.
8) Hisbergues M, Vendeville S, Vendeville P. Zirconia: Established facts and perspectives for a biomaterial in dental implantology. J Biomed Mater Res B 2009; 88: 519-529.
9) Gahlert M, Gudehus T, Eichhorn S, Steinhauser E, Kniha H, Erhardt W. Biomechanical and histomorphometric comparison between zirconia implants with varying surface textures and a titanium implant in the maxilla of miniature pigs. Clin Oral Impl Res 2007; 18: 662-668.
10) Yamashita D, Sato H, Miyamoto M, Machigashira M, Kanbara K, Ban S. Apatite coating on zirconia using glass coating technique. J Ceram Soc Jpn 2008; 116: 20-22.
11) Setzer B. Bächle M, Metzger MC, Kohal RJ. The gene-expression and phenotypic response of hFOB 1.19 osteoblasts to surface-modified titanium and zirconia. Biomaterials 2009; 30: 979-990.
12) Wurst JC, Nelson JA. Lineal intercept technique for measuring grain size in two-phase polycrystalline ceramics. J Am Ceram Soc 1972; 55: 109.
13) Mendelson MI. Average grain size in polycrystalline ceramics. J Am Ceram Soc 1969; 52: 443-446.
14) International Organization for Standardization. ISO 4049. Dentistry — Polymer-based filling, restorative and luting materials, 3rd ed, 2000.
15) International Organization for Standardization. ISO 9917-1. Dentistry − Water-based cements — Part 1: Powder/liquid acid-base cements, 2nd ed, 2007.
16) Davy KWM, Anseau MR, Berry C. Iodinated methacrylate copolymers as X-ray opaque denture base acrylics. J Dent 1997; 25: 499-505.
17) Sobokbar A, Fujikawa Y, Murray DW, Athanasou NA. Radio-opaque agents in bone cement increase bone resorption. J Bone Joint Surg 1997; 79-B: 129-134.
18) O'Rourke B, Walls AWG, Wassell RW. Radiographic detection of overhangs formed by resin composite luting agents. J Dent 1995; 23: 353-357.
19) Murty RC. Effective atomic numbers of heterogeneous materials. Nature 1965; 207: 398-399.
20) Weber J, van den Berge DJ. The effective atomic number and the calculation of the composition of phantom materials. Br J Radiol 1969; 42: 378-383.
21) Lide DR. Handbook of Chemistry and Physics on CD-ROM, Chapman and Hall/CRC, Boca Raton, 2002.